Percolation of binary disk systems: Modeling and theory

Kelsey Meeks,[1,2,*] John Tencer,[1] and Michelle L. Pantoya[2]
[1]*Sandia National Laboratories, Albuquerque, New Mexico 87123, USA*
[2]*Mechanical Engineering Department, Texas Tech University, Lubbock, Texas 79409-1021, USA*
(Received 14 July 2016; revised manuscript received 13 September 2016; published 12 January 2017)

The dispersion and connectivity of particles with a high degree of polydispersity is relevant to problems involving composite material properties and reaction decomposition prediction and has been the subject of much study in the literature. This work utilizes Monte Carlo models to predict percolation thresholds for a two-dimensional systems containing disks of two different radii. Monte Carlo simulations and spanning probability are used to extend prior models into regions of higher polydispersity than those previously considered. A correlation to predict the percolation threshold for binary disk systems is proposed based on the extended dataset presented in this work and compared to previously published correlations. A set of boundary conditions necessary for a good fit is presented, and a condition for maximizing percolation threshold for binary disk systems is suggested.

DOI: 10.1103/PhysRevE.95.012118

I. INTRODUCTION

For problems dealing with transport properties and particle connectivity, *percolation theory* is an important resource in predicting composite behavior. Percolation theory is the branch of statistical mechanics dealing with particle connectivity and dispersion in random media and provides a tool for linking microstructure and macroscopic material properties [1]. It is often described in terms of the critical parameter at which bulk connectivity is established, called the percolation threshold. Below the percolation threshold, large connected components do not exist.

Percolation is a well-studied physical phenomena because of its broad applicability, including physical percolation of fluids through rock [2–4], as well as resistor networks [5], disease spread [6], and many problems in material science [7,8]. Studies of these phenomena often focus on either lattice or continuum systems. Lattice percolation is described by regular or irregular networks, where sites or bonds are occupied with some probability f, and occupied sites form connected pathways. In the continuum, any point is available for occupancy, and the overlap and intersection of objects results in connected clusters. For either system, the problem of percolation can be summed up by the question: For a system of characteristic length L and a set of objects randomly located, what is the number, N, of objects necessary to create a connected cluster large enough to span the system? For the oft-studied infinite system, in which the intensive number of objects at percolation is also infinite, object occupancy is often described in terms of density, $n = N/L^2$ in two dimensions, or $n = N/L^3$ in three dimensions. In spite of the conceptual simplicity of this question, no exact solutions for any continuum percolation problems are yet known, although increasingly precise estimates have been obtained through extensive numerical simulation.

In 1970, Scher and Zallen demonstrated that for regular lattices there exists a universal critical area fraction for disks given by $\eta_{c,2} = 0.45$ and a critical volume fraction for spheres of $\eta_{c,3} = 0.16$ [9–11]. These quantities are invariant for all lattices that can be occupied by monodisperse disks or spheres, independent of specific lattice geometry and dependent only on the dimension of the system. Later work found percolation thresholds for systems of nonregular lattices [12–15]. Although lattice percolation has been the subject of much analytical and numerical study, continuum percolation is often more representative of the behavior of real systems [16–19].

For continuum percolation of monodisperse disks in two dimensions, it was discovered that the percolation threshold could be described by a universal total area fraction of 1.128 087 37 [20–22]. Further work showed that concept of a constant critical total area could be generalized to that of a universal total excluded area, and it was found that the excluded area of monodisperse objects is approximately constant at percolation, theorized to lie between 3.2 and 4.5 for any system of monodisperse objects in two dimensions [23]. Note that the total excluded area at percolation for monodisperse disks ($\sim$4.5) is consistent with the upper bound of the universal total excluded area range.

Several Monte Carlo methods have been used to predict percolation thresholds. Gradient percolation is a technique that simulates disks as centered on points of an underlying, inhomogeneous Poisson field [24]. The average location of the edge naturally formed by the percolating measure is used to compute the percolation threshold. Two techniques have been used to predict percolation thresholds in this manner: the gap-traversal method and the frontier-walk method. The frontier-walk method has been rigorously shown to converge to the percolation threshold for homogenous systems [25]. Other types of Monte Carlo methods include the rescaled-particle algorithm, in which a static particle configuration is rescaled to determine upper and lower percolation bounds [26] and several variations of the union-find algorithm [4,27,28], including one implementation adapted for use in the continuum by Mertens and Moore [20] based on the work Newman and Ziff [4].

These Monte Carlo simulations have been used to refine predictions of the percolation threshold of monodisperse disks [20–22], aligned squares [28,29], and sticks [20,27] to several decimal places of accuracy. Such simulations are costly and time consuming [24], but ever evolving computing

*Corresponding author: kmeeks@sandia.gov

 ©2017 American Physical Society

capabilities enable increasingly accurate and convenient simulations. However, the assumption of object monodispersion is often not accurate for physical systems [30–34]. This has driven several studies attempting to account for varying degrees of polydispersity in order to better transition theory to application.

Polydisperse systems have been demonstrated to have different percolation thresholds from monodisprse systems [31,35]. The problem of overlapping disks of two sizes in the continuum has been studied by several researchers. Quintanilla utilized extensive gradient Monte Carlo simulations to examine the percolation thresholds of such systems [24,36], including a proposed correlation for the percolation threshold as a function of disk radii ratio, λ, and relative concentration of the disk of smaller size, f. Based on those results, Balram and Dhar developed a phenomenological equation for the increase in the effective size of the larger disks in the presence of smaller disks [37]. Monte Carlo results have also predicted percolation thresholds for disks with distributions of radii [38]. The related problem for spheres of more than one size in three dimensions has also been examined [39,40]. The range of simulation results available over λ and f is limited, and few studies report results for values of λ less than 0.1 or values of f greater than 0.999. Although many of these works present potential extrapolation for some parameters, these extrapolations are often caveated outside of the simulation bounds.

Studies have also attempted to find the minimum or maximum percolation threshold for a set of conditions, as this is often physically relevant for problems such as determining how much additive is appropriate, as in the addition of carbon nanoparticles to a polymer composite [8], a maximum infection time for modeling of disease spread [6], or predicting the maximum set time before concrete becomes load bearing [41]. It has been proposed that for systems of disks, a monodispersion minimizes the percolation threshold [42,43]. It remains to be proven which conditions maximize the percolation threshold.

The objective of the present work is to extend the study of interpenetrating binary disk dispersions to higher polydispersities than considered previously and suggest a prediction of behavior. From these results, we propose criteria that will maximize the percolation threshold of such systems. This is a natural extension of the monodispersion studies previously reported and provides relevant simulations for applications that inherently include an additive with a size distribution.

II. METHODS

In this study, we use the union-find algorithm with open boundary conditions to determine the percolation threshold for binary disk dispersions for regions of high polydispersity, extending the results predicted by Monte Carlo simulation in the literature. This expanded data set is reported in full in Appendix. A discussion of the limiting behavior made evident by these expanded results, and a proposal for a new phenomenological equation for the prediction of percolation threshold for binary disk systems, is then put forth. We begin this discussion first with a definition of terms.

A. Definition of terms

The connectivity of objects can be described in terms of the filling factor, η which is the total area of all objects in a system normalized by system size. For a square domain with sides of length L, the filling factor for a system of N disks of radius R is given by

$$\eta = N\frac{\pi R^2}{L^2}. \tag{1}$$

The filling factor is often related to the area fraction, ϕ, which is the fraction of the domain covered by objects. The area fraction can also be thought of as the probability that any point in a domain is covered by an object. For lattice percolation, where objects do not overlap, the area fraction and filling factor are equivalent. However, for continuum percolation, in the case where interpenetration occurs, the area fraction will be less than the filling factor due to object overlap. The concepts of filling factor and area fraction can be directly extended to problems of three dimensions, where the filling factor is the total volume of all objects in the system normalized by system size and the volume fraction is the fraction of the domain covered by objects (equivalent to area fraction in two dimensions). In either case, as the domain size approaches infinity the area fraction is related to the total area by the differential equation $\frac{d\phi}{d\eta} = 1 - \phi$ which allows the solution

$$\phi = 1 - e^{-\eta}. \tag{2}$$

For the special case in which a system of objects has just achieved percolation, the area fraction is called the critical area fraction, or percolation threshold, ϕ_c. The corresponding filling fraction is called the critical filling fraction, η_c. For an infinite system, the probability that a cluster of connected objects results in connectivity across the domain goes from zero to one at the percolation threshold. In a finite system, like those we are able to simulate, the probability that such a cluster exists goes from zero, at the placement of the first object, to one as object placement causes the entire domain to be filled. This transition is continuous and becomes increasingly abrupt as the system grows in size, approaching an instantaneous transition for the infinite case.

For an infinitely large, two-dimensional system containing monodisperse disks (or equivalently for a system of finite size containing infinitesimally small monodisperse disks), the percolation threshold is an invariant, approximated by $\overline{\eta_c} = 1.128\,08$. This estimate was obtained independently via Monte Carlo methods using both gradient percolation [21] and wrapping probabilities [20].

B. Monte Carlo algorithm

In this work, Monte Carlo simulations are performed consistent with the spanning probability method used by Li and Zhang in [27]. In this approach, each simulation consists of a series of trials in which disks of a finite size are added to a much larger, finite 2D square. As each disk is placed, the Monte Carlo algorithm checks for overlap with other disks, merges connecting disks into clusters, and checks for a cluster that intersects two opposite sides of the domain. Such a cluster is called a spanning cluster, and its inception is congruous with the onset of percolation.

In each trial, the placement of disks continues until a spanning cluster has been found both horizontally and vertically. When a spanning cluster of each type first appears, the number of disks in the system is reported. For all system sizes, it is observed that the number of disks at which a horizontal spanning cluster appears and the number of disks at which a vertical spanning cluster appears are only weakly correlated. This is justified through an examination of results in this study and is consistent with assumptions made in the literature [20]. In this work, estimation of the monodisperse result consisted of O(10^5) trials. Estimates for binary disk systems consisted of O(10^3)-O(10^5) trials for each combination of f and λ, depending on the desired accuracy. The accuracy achieved for each data point is reflected in the number of significant figures reported in the Appendix.

Once both horizontal and vertical percolation has been achieved, the trial is ended and no more disks are placed. After performing a simulation consisting of m trials, the spanning probability $R_{N,L}$ for N disks in a system of size L is easily found by counting the total number of horizontal and vertical spanning events that occurred with fewer than N disks and dividing by $2m$. There is an obvious restriction in the resolution attainable for $R_{N,L}$ calculated in this manner for a given sample size, m. However, this difficulty may be overcome by convolving the measured spanning probabilities with the Poisson distribution with mean $\lambda = \eta(L^2/\pi R^2)$ [20,27], as shown in Eq. (3),

$$R_L(\eta) = \sum_{n=0}^{\infty} \frac{e^{\lambda}\lambda^n}{n!} R_{n,L}. \tag{3}$$

Following the work by Mertens and Moore [20], the Poisson weights $w_n \propto \frac{e^{-\lambda}\lambda^n}{n!}$ are calculated inductively to avoid numerical difficulties when n is large, as it is for any significant set of trials.

Calculation of w_n in this manner allows for a computationally accurate summation that does not involve summation of functionally infinite terms:

$$w_{\lfloor\lambda\rfloor-k} = \begin{cases} 0, & k = 0, \\ \frac{\lfloor\lambda\rfloor-(k-1)}{\lambda} w_{\lfloor\lambda\rfloor-(k-1)}, & k = 1,2,\ldots, \end{cases} \tag{4}$$

$$w_{\lfloor\lambda\rfloor+k} = \begin{cases} 1, & k = 0, \\ \frac{\lambda}{\lfloor\lambda\rfloor+k} w_{\lfloor\lambda\rfloor+(k-1)}, & k = 1,2,\ldots \end{cases} \tag{5}$$

The convolution is then normalized by the quantity $\sum w_n$. This technique allows for the computation of the spanning probability for any value of the filling factor. For the open boundary conditions considered here, the critical spanning probability is 0.5 [44]. The critical filling factor for a particular system size is defined as the filling factor at which the spanning probability is equal to the critical spanning probability for that size system. The critical filling factor for the finite system is expected to converge to that of the infinite system as $(R/L)^{7/4}$ [24]. Figure 1 illustrates that our algorithm converges at the expected rate.

The extrapolated value for the critical filling fraction is computed using a weighted linear regression as in [20,24]. The reported uncertainty in this prediction is the half-width of the 95% confidence interval for this prediction. For the monodisperse case, our prediction is $(1.1282 \pm 1.61) \times 10^{-4}$, which is in agreement with but less precise than the previously published values of 1.128 08 [21], 1.128 085 [36], and 1.128 087 37 [20]. This is to be expected as the present result was achieved with far fewer simulations as the goal of this work is not to refine the prediction for monodisperse disks but rather to explore the behavior of binary dispersions under extreme dispersiveness.

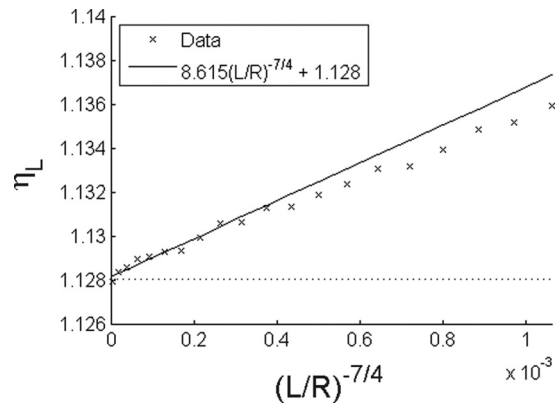

FIG. 1. Convergence of the estimated critical filling factor for monodisperse disks. Each data point represents a different relative system size (R/L). The fitted line to the data gives an intercept—or predicted percolation threshold for an infinite system—of 1.128, which demonstrates reasonably good agreement with the published percolation threshold value for monodisperse disks.

C. Checking against published results for monodisperse disks

To validate our implementation of the algorithm, this method is first used to determine the percolation threshold for monodisperse disks. Disks of size R were added to a square with side length L until both vertical and horizontal spanning clusters were observed. The number of disks necessary for percolation was recorded for each trial, and the resulting measured spanning probabilities were convolved with the Poisson distribution. This yielded an estimate of the two-dimensional percolation threshold for disks of $\overline{\eta_c} \approx (1.1282 \pm 1.61) \times 10^{-4}$, which is sufficiently precise for this study. The critical filling factor calculated for each simulation is shown in Fig. 1. System sizes below $R/L = 0.03$ were seen to be outside the asymptotic regime and therefore too small to yield useful information about the infinite percolation threshold.

III. RESULTS AND ANALYSIS

A. Presentation of results from Monte Carlo simulations

Having validated implementation of the Monte Carlo simulation method for the monodisperse case, we move to our particular case of interest: binary disk dispersions. Here, we are concerned with the effect of polydispersity on the percolation threshold for binary dispersions of fully penetrable disks of different radii. This system was studied previously by Quintanilla [24,36]. We adopt his notation, using $0 \leqslant \lambda \leqslant 1$ to denote the ratio of the disk radii and $0 \leqslant f < 1$ to denote the number fraction of the smaller disks. The number fraction is the concentration of small disks normalized by the total

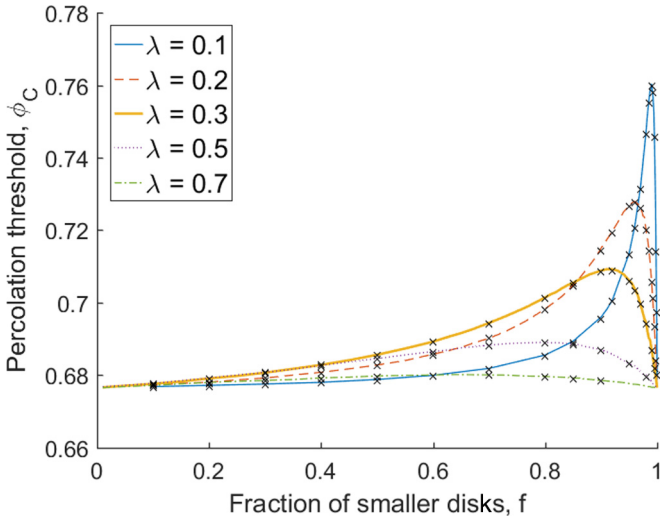

FIG. 2. Comparison of results generated here with those published by Quintanilla. The lines correspond to the points generated in this work while the x markers denote the corresponding results published in [24]. Very good agreement is demonstrated.

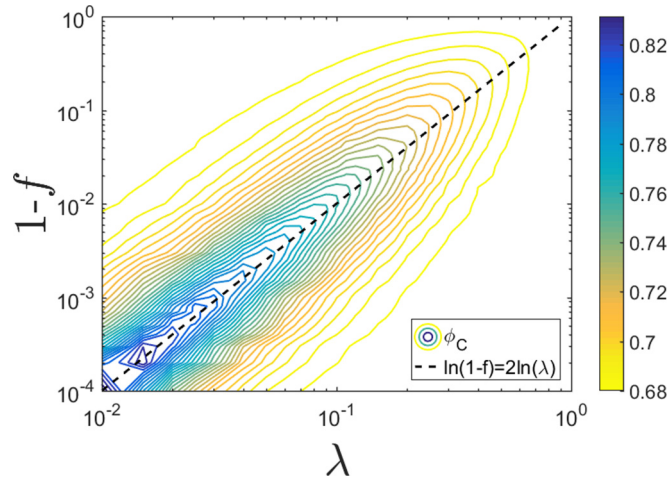

FIG. 3. Percolation threshold for binary dispersions of disks, presented as a contour plot. Each line represents a constant value of percolation thresholds. The dashed line closely tracks the location of the maximum percolation threshold.

number of disks and can also be thought of as the probability that a randomly selected disk is of the smaller size. We first verify our approach by reproducing Quintanilla's results.

Figure 2 shows Quintanilla's published results [24], as well as the results generated by the algorithm used in this paper. Very good agreement is demonstrated. All of the data points from [24] are reproduced and the maximum difference is $8.331\,264 \times 10^{-4}$ and the differences at each point are within the uncertainty bounds of our predictions. Although Quintanilla used a gradient percolation method, it is expected that both methods should converge to the same percolation threshold. Successfully reproducing these results provides confidence in our implementation. In this study, Quintanilla's results [24] have been extended for both smaller λ and larger f through extensive Monte Carlo simulations. Results from this study are reported in detail in the Appendix. Each value has an estimated error of $\leqslant 5$ in the last decimal place. The expanded dataset is used to generate Fig. 3—here presented in terms of $1 - f$ on a log-log scale—represents nearly five times the number of data points published by Quintanilla [24]. This expanded coverage is made possible both by the massive improvements in parallel computing since the publication of the prior work and by accepting slightly less precise solutions, particularly in regions far from the peak percolation threshold. Quintanilla and Ziff later published higher precision data [36] over roughly the same ranges of f and λ. Our uncertainties are large enough that there is no value in comparing to these results separately.

Our results are consistent with the previously proposed assertion that the minimum percolation threshold in two dimensions will be satisfied by monodisperse disks [24,36,39,42,43]. The results in Fig. 3 suggest that the percolation threshold will be maximized for smaller values of λ and some large value of f. The value of f for which the percolation threshold is maximized is dependent on the value of λ. Towards this end, it is instructive to consider the percolation threshold as a function of the large disk fraction, $1 - f$ instead of as a function of small disk fraction, f.

There are certain physical requirements for the limiting behavior of the percolation threshold for any set of dispersions. Here we used the simulation results as a tool to demonstrate the validity of such limits. As noted by Quintanilla [24], in the case where $f = 0$ or $\lambda = 1$, we expect that the percolation threshold should be equivalent to $\overline{\phi_c}$, as each of these systems represents the monodisperse case.

The extended Monte Carlo results also suggest several additional conditions for limiting behavior. Quintanilla [24,36] noted that the percolation threshold appeared to be maximum for small λ in the case of $(1 - f) \approx \lambda^2$. We further that observation by noting that not only does it hold true for the extended Monte Carlo results, but that consideration of limits supports this hypothesis. For a given ratio of radii, the maximum percolation threshold is achieved with a large disk number fraction of λ^2. Note that this hypothesis is distinct from the hypothesis that the percolation threshold be symmetric, i.e. $\phi_c(\frac{f\lambda^2}{f\lambda^2+1-f}) = \phi_c(\frac{1-f}{f\lambda^2+1-f})$ which was proposed in [45] and disproved in [36].

This is supported empirically by the Monte Carlo results but may be understood analytically by considering percolation of the binary disk mixture as two collocated percolating systems: a system of larger disks and a system of smaller disks. This ratio may be thought of as the total area of the large disks at percolation, normalized by the total area of all disks if all disks were of the smaller size. The total number of disks rather than the number of small disks is used in the denominator because there is effectively a small disk at the center of every large disk. Thus, the ratio is a measure of how close both systems are to percolation. The percolation threshold will be maximized when both systems contribute equally to percolation, and the ratio is unity, as in Eq. (6):

$$\frac{1-f}{\lambda^2} = \frac{(1-f)R^2 n_c}{\lambda^2 R^2 f n_c} = 1. \tag{6}$$

This result is also supported through the consideration of a pair of limiting cases. For the case in which both $(1-f)$ and λ approach zero, consider total area fraction for monodisperse disks shown in Eq. (7):

$$\eta_c = n_c(1-f)\pi R^2 + n_c f\lambda^2\pi R^2. \tag{7}$$

In this equation, the first term represents the contribution of the large disks to the total area, and the second term the contribution of the small disks to the total area. Supposing that λ^2 approaches zero very rapidly compared to $(1-f)$ and the disks of the larger size drive percolation, then bulk percolation will occur when the disks of the larger size percolate, as in Eq. (8):

$$\overline{\eta_c} \approx n(1-f)\pi R^2. \tag{8}$$

The total area fraction for the percolating system can be written as

$$\eta_c = \overline{\eta_c}\left(1 + \frac{f\lambda^2}{1-f}\right). \tag{9}$$

In the case where λ^2 does, in fact, approach zero very rapidly compared to $(1-f)$, the second term goes to zero and $\eta_c = \overline{\eta_c}$. However, in the case where λ^2 approaches zero at about the same rate as $(1-f)$, the second term will be equal to unity and $\eta_c = 2\overline{\eta_c}$.

Similarly, if $(1-f)$ approaches zero very rapidly compared to λ^2, we may use Eq. (10),

$$\overline{\eta_c} \approx nf\lambda^2\pi R^2, \tag{10}$$

and

$$\eta_c = \overline{\eta_c}\left(1 + \frac{f\lambda^2}{1-f}\right). \tag{11}$$

In the case where $(1-f)$ does, in fact, approach zero very rapidly compared to λ^2, the first term goes to zero and $\eta_c = \overline{\eta_c}$. However, in the case where λ^2 approaches zero at about the same rate as $(1-f)$, the second term will be equal to unity and $\eta_c = 2\overline{\eta_c}$.

This result suggests a few additional restrictions on the maximum percolation threshold: the maximum achievable critical filling factor for a binary dispersion of disks is double the critical filling factor for the monodisperse case and it is achieved only in the limit as $f \to 1$ and $\lambda^2 \to 0$ at equal rates.

This limit based approach to determining the maximum percolation threshold raises some interesting questions about how percolation thresholds are maximized for very polydisperse systems, namely: How would the percolation threshold be limited for systems with three or more sizes of disks? The approach presented here indicates that for such systems, percolation threshold will be maximized when all disks contribute equally to percolation, and the ratio of their contributions is unity. Whether increasingly polydisperse systems are limited in this manner is the subject of future study.

B. Evaluation of previously proposed fits

Several works in the literature have proposed fits to Monte Carlo data which predict the percolation threshold for binary disk dispersions. Based on the limiting behaviors discussed above, a list of criteria for the behavior of any equation predicting the percolation threshold of binary disk dispersions is compiled and presented in Table I.

The criteria listed as 1 and 2 were noted by Quintanilla [24] along with the observational remark that the maximum value of ϕ_c for small values of λ appeared to track well with $(1-f) \approx \lambda^2$.

Several correlations have been proposed to fit the percolation threshold surface as a function of λ and f, which can be evaluated based on the criteria enumerated in Table I.

Dhar [40] used a correlation length argument to derive the estimate in Eq. (12):

$$\eta_c(f,\lambda) \propto \frac{f\lambda^2 + (1-f)^2}{f\lambda^2 + (1-f)\lambda^{3/4}}. \tag{12}$$

When plotted over the range of λ and f considered here, the Dhar estimate demonstrated poor correlation to Monte Carlo results. We note that the Dhar correlation yields the monodisperse result when $\lambda = 1$, which satisfies condition 1, but fails to satisfy the additional six criteria.

Quintanilla [24] proposed an alternate empirical fit to the Dhar correlation [40] for the range of λ and f considered in his results. That empirical fit is shown in Eq. (13),

$$\eta_c(f,\lambda) \approx \overline{\eta_c}\frac{a(f\lambda^2 + 1 - f)}{a - f}, \tag{13}$$

where the critical filling factor for monodisperse disks is given by $\overline{\eta_c} = \eta_c(1,\lambda) = \eta_c(f,1) \approx 1.128\,087\,37$, and the parameter a is given by Eq. (14):

$$a = 1 + \frac{e^{6.8\lambda}}{115}. \tag{14}$$

TABLE I. Limiting criteria for percolation threshold estimates of bidisperse disks in 2D continuums.

Criteria	Percolation threshold	λ^2	$(1-f)$	Notes
1	$\eta_c = \overline{\eta_c}$	$=1$	All	Disks have equivalent radii; the system is monodisperse.
2	$\eta_c = \overline{\eta_c}$	All	$=1$	All disks are of the larger size; the system is monodisperse.
3	$\eta_c = \overline{\eta_c}$	$\neq 0$	$=0$	All disks are of the smaller size; the system is monodisperse.
4	$\eta_c = \overline{\eta_c}$	$=0$	$\neq 0$	Small disks have no area and do not contribute to the filling fraction; the system is monodisperse.
5	$\overline{\eta_c} \leqslant \eta_c \leqslant 2\overline{\eta_c}$	All	All	Percolation threshold binary disks bounded by $\overline{\eta_c}$ and $2\overline{\eta_c}$.
6	Maximized	Small	$= \lambda^2$	The maximum value of $\eta_c(\cdot,\lambda)$ will occur at $(1-f) \approx \lambda^2$.
7	$\to 2\overline{\eta_c}$	$\to 0$	$\to 0$	$\eta_c \to 2\overline{\eta_c}$ when $(1-f)$ and λ^2 approach 0 at equal rates.

It should be noted that Quintanilla [24] advises against using this correlation outside of the range $0.1 \leqslant \lambda \leqslant 0.9$ due to its empirical nature and certain limiting requirements. Quintanilla generated this empirical fit by optimizing estimates of the number density of the large disks at the percolation threshold:

$$\rho' = \frac{n_{\text{large}}}{L^2} = \frac{\eta}{\pi R^2}\frac{1-f}{f\lambda^2 + 1 - f}. \tag{15}$$

When evaluated in regards to the proposed criteria, we see this fit does quite well in meeting criteria 2 and 5, but fails to satisfy conditions 1, 3, 4, 6, and 7. Although fairly good at predicting the percolation threshold within the bounds of the simulated work, the Quintanilla fit requires increasingly large numbers of small disks to meet the maximum requirements. The performance of this fit—and several others—with regards to criteria 6 is shown in Fig. 4. Interestingly, many of these fits scale well with varying powers of λ. In the case of the Quintanilla fit, the required number fraction of small disks for the maximum percolation threshold at high values of λ is greater than one, as shown in Fig. 4, a clear violation of physical constraints. Additionally, because this fit does not satisfy criteria 5, the maximum discrepancy between its predictions and our numerical data is 0.8126. This is an unacceptably large error.

Quintanilla later suggested in [36] a fit for binary disk dispersions of the form

$$\eta_c = \overline{\eta_c} + a(\lambda)\nu^{b(\lambda)}(1-\nu)^{c(\lambda)}. \tag{16}$$

Note that Eq. (16) includes a correction to a typo found in [36] where the "+" sign is missing. Equation (16) is proportional to the probability density function of the β distribution with parameters $b(\lambda)$ and $c(\lambda)$. Equation (16) trivially satisfies criteria 2 and 3. Provided $a(0) = a(1) = 0$, criteria 1 and 4 are satisfied as well. The location of the maximum value of $\eta_c(:,\lambda)$ is given by

$$\nu * (\lambda) = \frac{b(\lambda)}{b(\lambda) + c(\lambda)}. \tag{17}$$

Because the parameters were fit independently for each value of λ, the location of the maximum percolation threshold for this fit matches the experimental data very well. Unfortunately, the parameters $a(\lambda)$, $b(\lambda)$, and $c(\lambda)$ given in [36] are tabular and cannot be expanded outside of the range of λ considered in that work. This makes it impossible to verify criteria 5 or 7 or to look at criteria 6 rigorously, although the minimum prescribed in criteria 5 is satisfied. Because this fit cannot be used to extrapolate outside the range of λ used to generate it, we will not discuss it further.

In Meeks *et al.* [46], the concept of excluded area was generalized to polydisperse systems to predict percolation thresholds, and a new correlation of binary disk percolation was proposed, given by Eq. (18):

$$\eta_c = \frac{2\overline{\eta_c}[f\lambda^2 + (1-f)]}{[(\lambda^2 - 2\lambda + 1)f^2 + (\lambda^2 + 2\lambda - 3)f + 2]}. \tag{18}$$

It was noted that this fit—hereafter referred to as the "average excluded area prediction"—had moderately good agreement with the simulation results, satisfying criteria 1, 2, and 3. However, the average excluded area prediction does not recover condition 4, as in the case where $\lambda = 0$, the quantity η_c is undefined. It performs reasonably well at predicting maximum percolation thresholds, satisfying conditions 5 and 7, although it consistently overpredicted the location of the maximum percolation threshold for binary disk systems failing to satisfy criteria 6. Here we add that for a fixed ratio of radii, λ the number fraction of large disks corresponding to the maximum percolation threshold is observed to scale with λ rather than λ^2, as shown in Fig. 4. Because the average excluded area prediction satisfies criteria 5 but fails to satisfy criteria 6 the maximum discrepancy between its predictions and our numerical data approaches the range of values permitted by criteria 5 of 0.2189. The largest observed discrepancy was 0.2057. It is expected that this value should grow with the degree of polydispersity considered.

Meeks *et al.* [46] suggested a density factor to improve correlation, which here we refer to as γ, to be inserted in place of f. It was suggested that a correction factor for the density of the smaller disks would proportionally bias their contribution to the percolation threshold in a way that more accurately predicted the percolation threshold. For the corrected fit presented there, γ was equal to the small disk area fraction v, a quantity given by Eq. (19):

$$\gamma = v = \frac{f\lambda^2}{f\lambda^2 + (1-f)}. \tag{19}$$

This substitution was enacted such that a corrected correlation was proposed as Eq. (20):

$$\eta_c = \frac{2\overline{\eta_c}[v\lambda^2 + (1-v)]}{[(\lambda^2 - 2\lambda + 1)v^2 + (\lambda^2 + 2\lambda - 3)v + 2]}. \tag{20}$$

This "v-for-f substitution prediction" performs similarly to the average excluded area prediction, as it satisfies 1, 2, 3, 5, and 7 and fails to satisfy condition 4. This modified fit was

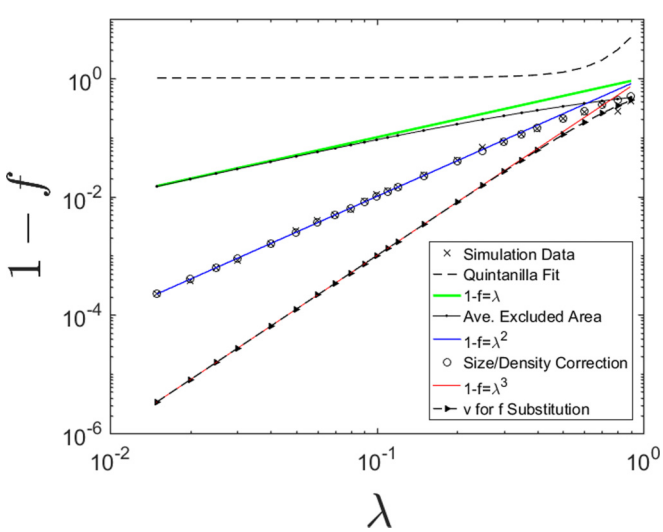

FIG. 4. Number density of large disks $(1-f)$ at the maximum percolation threshold, as a function of λ. Location of maximum percolation threshold as predicted by Monte Carlo simulation, the v-for-f substitution and average excluded area predictions, the empirical fit proposed by Quintanilla [24], and the correlation proposed in this work.

noted to predict percolation threshold far from the peak much more accurately than the average excluded area prediction. Although, the v-for-f substitution prediction predicts the location of the maximum percolation threshold much more accurately than the average excluded area prediction, it consistently overpredicts this value, as shown in Fig. 4—scaling with λ^3 rather than the previous λ or the desired λ^2—and thus does not fully satisfy condition 6. The maximum observed discrepancy for this fit was 0.1645 over the range of f and λ considered but it is expected to approach 0.2189 for larger values of f and smaller values of λ in the same way as the average excluded area prediction.

C. Proposal of a new correlation for prediction of percolation threshold

Given the ability of the Meeks correlation to satisfy nearly all of the limiting criteria, we naturally ask if additional adjustments can be made to the structure of that fit which will allow us to satisfy conditions 4 and 6. Based on the approach in [46], we propose a correlation with a density correction factor, γ, as well as a size-correction factor given by β, which can be inserted into Eq. (18) in place of f and λ, respectively, leading to a correlation which takes the form

$$\eta_c = \frac{2\overline{\eta_c}[\gamma\beta^2 + (1-\gamma)]}{[(\beta^2 - 2\beta + 1)\gamma^2 + (\beta^2 + 2\beta - 3)\gamma + 2]}. \tag{21}$$

Note that the v-for-f substitution prediction in Eq. (20) takes exactly this form, with $\beta = \lambda$ and $\gamma = v$. Here we propose another fit of this form, with a size-correction factor shown in Eq. (22),

$$\beta = \lambda^{2/3}, \tag{22}$$

and a density correction factor shown in Eq. (23):

$$\gamma = \frac{f\lambda^2}{f\lambda^2 + (1-f)^{3/2}}. \tag{23}$$

This correlation, since γ and β collapse to f and λ in the degenerate cases of $f = 0$ and $\lambda = 1$, maintains the same limiting conditions in those scenarios as Eq. (18). As such, this correlation satisfies conditions 1, 2, 3, 5, and 7 in exactly the same way as the v-for-f substitution prediction given by Eq. (20). The degenerate case of $\lambda = 0$ now reduces to the monodisperse result, satisfying condition 4. We now check the location of the maxima, shown in Fig. 6, and observe very good agreement with the simulation results, satisfying condition 6. The maximum observed discrepancy for this fit was 0.0723 over the range of f and λ considered, and, unlike the other fits, this value is not expected to increase for larger values of f and smaller values of λ since this fit satisfies all of the limiting criteria.

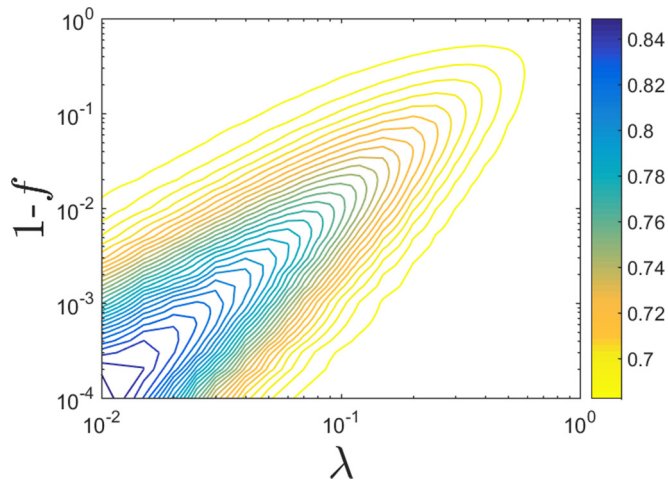

FIG. 5. Percolation threshold predicted by size-density correlation given by Eqs. (21)–(23). Contour plot for all considered number fractions and radii ratios. This plot demonstrates a high degree of similarity to the simulation data presented in Fig. 3

For a given ratio of disk radii, λ, the value of f for which the percolation threshold is maximized may be determined from any of these fits quite easily. For the Quintanilla fit [24], this maximum lies outside of the acceptable range of f. Specifically, $\eta_c(f;\lambda)_f = \max \eta_c \Rightarrow f < 0$. Figure 4 shows the differences between the locations of the maximums predicted by the various fits and simulation data. The proposed relation that $1 - f = \lambda^2 \Rightarrow \eta_c(f,\lambda) = \max_{f,\lambda} \eta_c$ agrees very well with the simulation data.

From Fig. 4 we make a few interesting observations. Condition 6 proposes that the maximum percolation threshold for bidisperse disks will occur when $1 - f = \lambda^2$ and that the best predictors of percolation threshold will conform to this condition. The simulation data and correlation proposed by Eqs. (21)–(23) adhere to this condition very well. Although the v-for-f substitution prediction and average excluded area prediction do not closely scale with λ^2, interestingly, they scale very well with λ^3 and λ, respectively. The reason for this behavior is not yet known; however, it indicates that the constant excluded volume approach to prediction of percolation thresholds detailed by [46] has excellent potential to capture a wide range of behaviors for polydisperse systems.

The performance of the proposed fit can be further compared to the simulation results. Figure 5 shows a contour plot of the percolation threshold predicted by Eqs. (21)–(23). While not a perfect fit, the proposed correlation matches the simulation data (Fig. 3) quite well over the entire range of λ and f considered. Taken with its satisfaction of all of the limiting cases, it is expected that the proposed fit may be used to predict percolation thresholds for bidisperse systems somewhat beyond the range of values simulated. The close resemblance between Fig. 5 and Fig. 3 indicates that the correlation proposed by Eqs. (21)–(23) predicts the behavior of the percolation threshold very well, even in regions far from the end conditions. By quantitatively comparing the results from the simulation data detailed in the Appendix to the percolation thresholds predicted by the

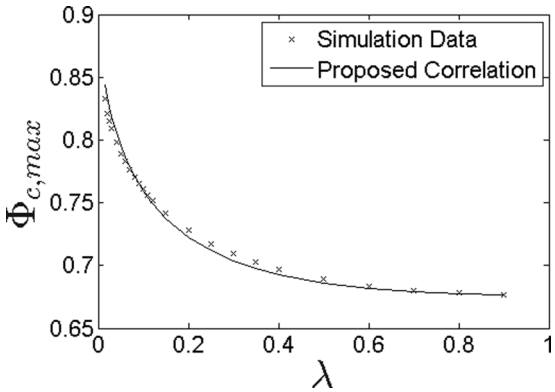

FIG. 6. The maximum percolation threshold predicted for binary disk dispersions for both the simulation data and the proposed correlation given by Eqs. (21)–(23). Very good agreement is demonstrated, and the values predicted by the proposed correlation match the simulation data to within 2%.

correlation, we note that the values predicted by the proposed correlation are within 13% of the value found by the simulation in all regions and are within 3% when λ is greater than 0.1 and f is less than 0.97. This is consistent with good agreement in all regions and excellent agreement in regions of lower polydispersity.

There is a plethora of ways in which the performance of the correlation proposed by Eqs. (21)–(23) can be compared to the simulation data enumerated in the Appendix. Although an exhaustive quantification of the similarity would perhaps be somewhat tedious, and certainly beyond the scope of this work, one such comparison is shown in Fig. 6. Figure 6 depicts the behavior maximum predicted percolation threshold as a function of λ for both the proposed correlation and the simulation data. Figure 6 shows a quantity of interest for this work—namely the maximum possible percolation threshold for a given value of λ—for both the proposed correlation and the simulation data. The predicted values correspond to within 2%, demonstrating excellent agreement. Such comparisons show quantitatively that the correlation given in Eqs. (21)–(23) performs quite well in predicting quantities of particular interest, even in the presence of very high polydispersity.

IV. CONCLUSIONS

In this work we examined the effect of very high polydispersity on the percolation threshold for binary disk systems. This work confirmed Quintanilla's binary disk results [24,36] and expanded the simulation regime to include nearly 5 times as many data points over a much larger range of disk radii ratio, λ, and small disk concentration, f. This work proposes that the maximum percolation threshold for a binary disk system will be achieved when $(1-f) \approx \lambda^2$ and that the percolation threshold for any binary disk dispersion cannot exceed $2\overline{\eta_c}$. A set of criteria for fits predicting the percolation threshold for binary disk dispersions is proposed, and a new fit satisfying all proposed conditions is put forth.

ACKNOWLEDGMENTS

Sandia National Laboratories is a multiprogram laboratory managed and operated by Sandia Corporation, a wholly owned subsidiary of Lockheed Martin Corporation, for the U.S. Department of Energy's National Nuclear Security Administration under Contract No. DE-AC04-94AL85000. This document has been reviewed and approved for unclassified, unlimited release under 2015-475586. The authors are grateful for additional support by the Army Research Office under Contract No. W911NF-11-1-0439 and encouragement by our program manager, Dr. Ralph Anthenien.

APPENDIX

This appendix contains the values of the percolation threshold predicted by the Monte Carlo simulations. Results from this study are reported in detail in the Appendix. Each value has an estimated error of $\leqslant 5$ in the last decimal place. Table II contains the simulation results for low values of f and low values of λ and covers much of the same range examined by Quintanilla [24]. Table III shows the simulation results for low values of f and high values of λ. Table IV shows the simulation results for the region of highest polydispersity with high values of f and low values of λ. Table V shows the simulation results for high values of f and high values of λ.

TABLE II. Simulation results for low values of f and low values of λ.

		Radius ratio (λ)									
		0.01	0.02	0.03	0.04	0.05	0.06	0.07	0.08	0.09	0.1
Small disk number density (f)	0.10	0.6765	0.6765	0.6766	0.6766	0.6766	0.6766	0.6767	0.6767	0.6767	0.6768
	0.20	0.6766	0.6766	0.6766	0.6767	0.6768	0.6768	0.6769	0.6770	0.6771	0.6771
	0.30	0.6765	0.6766	0.6766	0.6767	0.6768	0.6769	0.6770	0.6771	0.6773	0.6775
	0.40	0.6765	0.6766	0.6766	0.6768	0.6769	0.6771	0.6773	0.6775	0.6778	0.6780
	0.50	0.6765	0.6767	0.676 81	0.6770	0.6772	0.6775	0.6777	0.6781	0.6784	0.6788
	0.60	0.6766	0.6767	0.6769	0.6771	0.6775	0.6779	0.6784	0.6789	0.6793	0.6799
	0.70	0.6768	0.6769	0.6773	0.6778	0.6783	0.6788	0.6795	0.6803	0.6811	0.6819
	0.80	0.6767	0.6771	0.6777	0.6785	0.6793	0.6803	0.6815	0.6828	0.6841	0.6854
	0.85	0.6768	0.6774	0.6782	0.6793	0.6805	0.6818	0.6836	0.6854	0.6871	0.6891

TABLE III. Simulation results for low values of f and high values of λ.

Small disk number density (f)	Radius ratio (λ)											
	0.12	0.15	0.2	0.25	0.3	0.35	0.4	0.5	0.6	0.7	0.8	0.9
0.01	0.6766	0.6765	0.6767	0.6767	0.6767	0.6767	0.6768	0.6769	0.6766	0.6765	0.6768	0.6768
0.10	0.6769	0.6770	0.6772	0.6774	0.6776	0.6777	0.6778	0.6777	0.6775	0.6773	0.6769	0.6765
0.15	0.6770	0.6773	0.6777	0.6780	0.6783	0.6785	0.6786	0.6785	0.6781	0.6775	0.6770	0.6766
0.20	0.6773	0.6776	0.6781	0.6786	0.6791	0.6792	0.6794	0.6793	0.6787	0.6780	0.6772	0.6766
0.25	0.6775	0.6780	0.6787	0.6793	0.6798	0.6802	0.6803	0.6801	0.6793	0.6783	0.6774	0.6768
0.30	0.6778	0.6784	0.6792	0.6800	0.6807	0.6811	0.6812	0.6808	0.6799	0.6786	0.6775	0.6766
0.35	0.6782	0.6788	0.6800	0.6809	0.6817	0.6822	0.6823	0.6817	0.6803	0.6788	0.6777	0.6768
0.40	0.6786	0.6794	0.6808	0.6820	0.6828	0.6833	0.6835	0.6827	0.6810	0.6792	0.6777	0.6768
0.45	0.6791	0.6801	0.6817	0.6833	0.6841	0.6846	0.6847	0.6836	0.6816	0.6795	0.6778	0.6769
0.50	0.6795	0.6808	0.6828	0.6845	0.6856	0.6862	0.6861	0.6846	0.6821	0.6799	0.6779	0.6768
0.55	0.6803	0.6817	0.6841	0.6860	0.6873	0.6879	0.6876	0.6856	0.6826	0.6799	0.6781	0.6768
0.60	0.6812	0.6829	0.6857	0.6879	0.6892	0.6896	0.6893	0.6865	0.6830	0.6801	0.6779	0.6769
0.63	0.6817	0.6836	0.6868	0.6892	0.6907	0.6909	0.6903	0.6871	0.6833	0.6801	0.6780	0.6768
0.64	0.6819	0.6839	0.6873	0.6898	0.6911	0.6914	0.6906	0.687 29	0.6834	0.6802	0.6780	0.6768
0.65	0.6821	0.6843	0.6876	0.6902	0.6917	0.6918	0.6910	0.6875	0.6835	0.6802	0.6779	0.6768
0.67	0.6828	0.6851	0.6886	0.6914	0.6926	0.6928	0.6917	0.6878	0.6835	0.680 14	0.6780	0.6769
0.70	0.6836	0.6862	0.6902	0.6932	0.6944	0.6941	0.6928	0.6883	0.6835	0.6800	0.6779	0.6768
0.73	0.6846	0.6877	0.6921	0.6952	0.6963	0.6958	0.6938	0.6887	0.6836	0.6800	0.6780	0.6769
0.75	0.6855	0.6887	0.6936	0.6967	0.6976	0.6967	0.6946	0.6888	0.6836	0.6799	0.6778	0.6769
0.77	0.6865	0.6901	0.6952	0.6983	0.6990	0.6978	0.6952	0.6890	0.6835	0.6798	0.6778	0.6768
0.80	0.6884	0.6925	0.6981	0.7012	0.7014	0.6994	0.6961	0.6891	0.6833	0.6797	0.6777	0.6767
0.81	0.6891	0.6934	0.6993	0.7023	0.7022	0.6999	0.6964	0.6889	0.6832	0.6796	0.6777	0.6767
0.82	0.6899	0.6944	0.7005	0.7034	0.7030	0.7004	0.6967	0.6889	0.6831	0.6795	0.6775	0.6767
0.83	0.6909	0.6957	0.7018	0.7047	0.7038	0.7009	0.6968	0.6888	0.6830	0.6794	0.6775	0.6767
0.84	0.6916	0.6967	0.7031	0.7057	0.7047	0.7013	0.69696	0.6887	0.6828	0.6794	0.6775	0.6768
0.85	0.6929	0.6981	0.7048	0.7070	0.7054	0.7017	0.6970	0.6885	0.6826	0.6793	0.6775	0.6767
0.86	0.6941	0.6997	0.7064	0.7083	0.7063	0.7021	0.6971	0.6883	0.6825	0.6792	0.6774	0.6767
0.87	0.6955	0.7016	0.7082	0.7097	0.7069	0.7022	0.6969	0.6880	0.6822	0.6789	0.6773	0.6767
0.88	0.6972	0.7034	0.7101	0.7111	0.7077	0.7023	0.6968	0.687 70	0.6820	0.6789	0.6772	0.6767
0.89	0.6990	0.7056	0.7124	0.7125	0.7083	0.7024	0.6965	0.6874	0.6817	0.6787	0.6772	0.6767

TABLE IV. Simulation results for high values of f and low values of λ.

	Radius ratio (λ)											
Small disk number density (f)	0.01	0.015	0.02	0.025	0.03	0.04	0.05	0.06	0.07	0.08	0.09	0.1
0.9	0.677	0.6773	0.6780	0.6783	0.6790	0.6808	0.6828	0.6851	0.6876	0.6903	0.6930	0.6958
0.91	0.678	0.678	0.679	0.679	0.680	0.681	0.684	0.686	0.689	0.692	0.695	0.6978
0.92	0.677	0.678	0.6781	0.679	0.6801	0.6820	0.6845	0.6874	0.6905	0.6940	0.697	0.7005
0.95	0.677	0.678	0.679	0.680	0.6819	0.6852	0.6893	0.6940	0.6988	0.7038	0.7087	0.7133
0.96	0.678	0.6785	0.6795	0.6811	0.6831	0.6873	0.6925	0.6983	0.7040	0.7100	0.7155	0.7209
0.97	0.678	0.679	0.6809	0.6831	0.685	0.6909	0.6980	0.7052	0.7124	0.7198	0.7260	0.7315
0.98	0.679	0.681	0.6828	0.686	0.6897	0.698	0.7077	0.7174	0.7271	0.7355	0.7421	0.7466
0.983					0.6918	0.7015	0.713		0.734	0.743	0.749	0.7527
0.985									0.7400	0.748	0.754	0.7556
0.9875									0.748	0.7556	0.7591	0.7586
0.99	0.680	0.684	0.688	0.695	0.702	0.718	0.733	0.7475	0.758	0.7634	0.7638	0.7602
0.991									0.762	0.7666	0.7652	0.758
0.992	0.682		0.692	0.701	0.708	0.726	0.7449	0.759	0.7671	0.7689	0.7652	0.7577
0.993								0.766	0.770	0.769	0.7641	0.754
0.994							0.763	0.773	0.774	0.771	0.761	0.752
0.995	0.683	0.692	0.702	0.713	0.725	0.751	0.770	0.778	0.7764	0.7678	0.7567	0.7458
0.996							0.780	0.783	0.7741			
0.997	0.688		0.715	0.731	0.751	0.779	0.789	0.781	0.7657	0.7512	0.7383	0.7276
0.9975						0.786	0.789	0.777				
0.998					0.775	0.795	0.786					
0.9985					0.793	0.798	0.776					
0.999	0.712	0.744	0.777	0.800	0.807	0.785	0.756	0.735	0.7203	0.710	0.7028	0.6973
0.9991				0.808	0.808	0.781						
0.9992			0.792	0.813	0.809	0.774						
0.9993	0.723	0.763	0.796	0.813	0.804							
0.9994			0.809	0.815	0.797							
0.9995	0.739	0.785	0.815	0.810	0.786							
0.9996		0.803	0.821	0.799								
0.9997	0.771	0.825	0.815	0.782	0.756	0.724	0.707	0.6978	0.692	0.688	0.6849	0.6837
0.9998	0.808	0.831	0.790									
0.9999	0.836	0.786	0.743	0.722	0.707	0.6942	0.687	0.684	0.6817	0.680	0.6794	0.6788

TABLE V. Simulation results for high values of f and high values of λ.

Small disk number density (f)	Radius ratio (λ)												
	0.11	0.12	0.15	0.2	0.25	0.3	0.35	0.4	0.5	0.6	0.7	0.8	0.9
0.9	0.6984	0.7013	0.7083	0.7147	0.7140	0.7087	0.7023	0.6961	0.6869	0.6815	0.6786	0.6772	0.6766
0.91	0.702	0.704	0.711	0.7173	0.7150	0.7090	0.7019	0.6956	0.6864	0.6811	0.6784	0.6771	0.6766
0.92	0.705	0.7068	0.7147	0.7195	0.7162	0.7091	0.7012	0.6948	0.6857	0.6808	0.6782	0.6770	0.6766
0.93	0.707	0.713	0.7185	0.7222	0.7171	0.7085	0.7004	0.6940	0.685	0.6803	0.6781	0.6770	0.6766
0.94	0.7118	0.716	0.7231	0.7248	0.7172	0.7077	0.699	0.6927	0.6841	0.6800	0.6780	0.6769	0.6765
0.95	0.719	0.7214	0.7282	0.7267	0.7167	0.7062	0.6974	0.6912	0.6832	0.6795	0.6777	0.6769	0.6766
0.955	0.724	0.726	0.732	0.7273	0.716	0.705	0.697	0.690	0.6827	0.6792	0.6775	0.6769	0.6765
0.96	0.7256	0.7289	0.7341	0.7277	0.7148	0.7036	0.6952	0.6892	0.6824	0.6790	0.6775	0.6768	0.6765
0.965	0.732	0.734	0.737	0.7272	0.714	0.702	0.694	0.688	0.6818	0.6787	0.6774	0.6767	0.6765
0.97	0.737	0.7386	0.7393	0.7263	0.7115	0.6997	0.6919	0.6868	0.6810	0.6784	0.6773	0.6767	0.6765
0.975	0.741	0.744	0.7410	0.724	0.709	0.697	0.6901	0.685	0.6804	0.6781	0.6771	0.6767	0.6766
0.977	0.747	0.747	0.7413	0.724	0.707	0.696	0.689	0.685	0.6802	0.6779	0.6771	0.6766	0.6766
0.98	0.7491	0.7489	0.7408	0.7202	0.7045	0.6943	0.6881	0.6841	0.6799	0.6778	0.676 94	0.6766	0.6766
0.983	0.7521	0.7511	0.7392	0.717	0.703	0.692	0.687	0.683	0.6792	0.6776	0.676 86	0.6766	0.6765
0.985	0.7544	0.7517	0.7375	0.715	0.700	0.690	0.686	0.681	0.6791	0.6775	0.6768	0.6765	0.6766
0.9875	0.7559	0.7511	0.735	0.711	0.697	0.6896	0.6856	0.681	0.6789	0.6773	0.6768	0.6765	0.6765
0.99	0.7546	0.7478	0.7282	0.7058	0.6936	0.6868	0.6828	0.6807	0.6782	0.6772	0.6767	0.6765	0.676 49
0.992	0.751	0.743	0.721	0.7010	0.692	0.6849	0.683	0.6798	0.6778	0.6770	0.6767	0.6765	0.6765
0.995	0.737	0.728	0.709	0.692	0.686	0.6820	0.680	0.6786	0.6773	0.6768	0.6766	0.6765	0.6764
0.997	0.720	0.7123	0.6988	0.6878	0.682	0.6799	0.678	0.6779	0.6770	0.6766	0.6765	0.6765	0.6765
0.998	0.708	0.702	0.6917	0.6842	0.681	0.6785	0.678	0.678	0.677	0.6766	0.6765	0.6765	0.6765
0.999	0.6939	0.6902	0.6848	0.6806	0.678	0.6777	0.677	0.6769	0.6767	0.6765	0.6765	0.6764	0.6765
0.9997	0.682	0.681	0.6791	0.6784	0.677	0.6765	0.676	0.677	0.677	0.6765	0.6765	0.6764	0.6765
0.9999	0.678	0.678	0.677	0.6773	0.677	0.6766	0.6765	0.6765	0.6764	0.6764	0.6765	0.6764	0.6765

[1] Jie Liu and Klaus Regenauer-Lieb, Application of percolation theory to microtomography of structured media: Percolation threshold, critical exponents, and upscaling, Phys. Rev. E **83**, 016106 (2011).

[2] E. N. Gilbert, Random plane networks, J. Soc. Ind. Appl. Math. **9**, 533 (1961).

[3] M. Sahimi, Long-range correlated percolation and flow and transport in heterogeneous porous media, J. Phys. I **4**, 1263 (1994).

[4] M. E. J. Newman and R. M. Ziff, Fast Monte Carlo algorithm for site or bond percolation, Phys. Rev. E **64**, 016706 (2001).

[5] L. DeArcangelis, S. Redner, and A. Coniglio, Anomalous voltage distribution of random resistor networks and a new model for the backbone at the percolation-threshold, Phys. Rev. B **31**, 4725 (1985).

[6] Fabricio Benevides and M. Przykucki, Maximum percolation time in two-dimensional bootstrap percolation, SIAM J. Discrete Math. **29**, 1 (2015).

[7] Dylan K. Smith and Michelle L. Pantoya, Effect of nanofiller shape on effective thermal conductivity of fluoropolymer composites, Compos. Sci. Technol. **118**, 251 (2015).

[8] Ahmet Sari and Ali Karaipekli, Thermal conductivity and latent heat thermal energy storage characteristics of paraffin/expanded graphite composite as phase change material, Appl. Therm. Eng. **27**, 1271 (2007).

[9] Harvey Scher and Richard Zallen, Critical density in percolation processes, J. Chem. Phys. **53**, 3759 (1970).

[10] M. E. J. Newman and R. M. Ziff, Efficient Monte Carlo Algorithm and High-Precision Results for Percolation, Phys. Rev. Lett. **85**, 4104 (2000).

[11] Richard Zallen and Harvey Scher, Percolation on a continuum and the localization-delocalization transition in amorphous semiconductors, Phys. Rev. B **4**, 4471 (1971).

[12] Chengxiang Ding, Zhe Fu, Wenan Guo, and F. Y. Wu, Critical frontier of the Potts and percolation models on triangular-type and kagome-type lattices. II. Numerical analysis, Phys. Rev. E **81**, 061111 (2010).

[13] O. Melchert, Helmut G. Katzgraber, and M. A. Novotny, Site- and bond-percolation thresholds in $\boldsymbol{K}_{n,n}$-based lattices: Vulnerability of quantum annealers to random qubit and coupler failures on chimera topologies, Phys. Rev. E **93**, 042128 (2016).

[14] Richard A. Neher, Klaus Mecke, and Herbert Wagner, Topological estimation of percolation thresholds, J. Stat. Mech.: Theory Exp. (2008) P01011.

[15] S. N. Dorogovtsev, A. V. Goltsev, and J. F. F. Mendes, Critical phenomena in complex networks, Rev. Mod. Phys. **80**, 1275 (2008).

[16] Sang Bub Lee and S. Torquato, Monte Carlo study of correlated continuum percolation: Universality and percolation thresholds, Phys. Rev. A **41**, 5338 (1990).

[17] A. L. R. Bug, S. A. Safran, and I. Webman, Continuum Percolation of Rods, Phys. Rev. Lett. **54**, 1412 (1985).

[18] L. M. Schwartz, F. Auzerais, J. Dunsmuir, N. Martys, D. P. Bentz, and S. Torquato, Transport and diffusion in

three-dimensional composite media, Physica A **207**, 28 (1994).

[19] A. M. S. Tremblay and J. MacHta, Finite-size effects in continuum percolation, Phys. Rev. B **40**, 5131 (1989).

[20] Stephan Mertens and Cristopher Moore, Continuum percolation thresholds in two dimensions, Phys. Rev. E **86**, 061109 (2012).

[21] J. Quintanilla, S. Torquato, and R. M. Ziff, Efficient measurement of the percolation threshold for fully penetrable discs, J. Phys. A: Math. Gen. **33**, L399 (2000).

[22] E. T. Gawlinski and H. E. Stanley, Continuum percolation in two dimensions: Monte Carlo tests of scaling and universality for non-interacting discs, J. Phys. A: Math. Gen. **14**, L291 (1981).

[23] I. Balberg, C. H. Anderson, S. Alexander, and N. Wagner, Excluded volume and its relation to the onset of percolation, Phys. Rev. B **30**, 3933 (1984).

[24] J. Quintanilla, Measurement of the percolation threshold for fully penetrable disks of different radii, Phys. Rev. E **63**, 061108 (2001).

[25] S. Zuyev and J. Quintanilla, Estimation of percolation thresholds via percolation in inhomogeneous media, J. Math. Phys. **44**, 6040 (2003).

[26] S. Torquato and Y. Jiao, Effect of dimensionality on the continuum percolation of overlapping hyperspheres and hypercubes. II. Simulation results and analyses, J. Chem. Phys. **137**, 074106 (2012).

[27] J. Li and S.-L. Zhang, Finite-size scaling in stick percolation, Phys. Rev. E **80**, 040104(R) (2009).

[28] Don R. Baker, Gerald Paul, Sameet Sreenivasan, and H. Eugene Stanley, Continuum percolation threshold for interpenetrating squares and cubes, Phys. Rev. E **66**, 046136 (2002).

[29] Paul Balister, Béla Bollobás, and Mark Walters, Continuum percolation with steps in an annulus, Ann. Appl. Prob. **14**, 1869 (2004).

[30] E. Vargas, M. L. Pantoya, M. A. Saed, and B. L. Weeks, Advanced susceptors for microwave heating of energetic materials, Mater. Des. **90**, 47 (2016).

[31] M. K. Phani and D. Dhar, Continuum percolation with discs having a distribution of radii, J. Phys. A: Math. Gen. **17**, L645 (1984).

[32] J. J. Moore and H. J. Feng, Combustion synthesis of advanced materials: Part I. Reaction parameters, Prog. Mater. Sci. **39**, 243 (1995).

[33] N. Yoshikawa, K. Kawahira, Y. Saito, H. Todoroki, and S. Taniguchi, Estimation of microwave penetration distance and complex permittivity of graphite by measurement of permittivity and direct current conductivity of graphite powder mixtures, J. Appl. Phys. **117**, 084105 (2015).

[34] Michael Ibrahim, Maria Bassil, Umit B. Demirci, Tony Khoury, Georges El Haj Moussa, Mario El Tahchi, and Philippe Miele, Polyaniline–titania solid electrolyte for new generation photovoltaic single-layer devices, Mater. Chem. Phys. **133**, 1040 (2012).

[35] B. Lorenz, I. Orgzall, and H. O. Heuer, Universality and cluster structures in continuum models of percolation with two different radius distributions, J. Phys. A: Math. Gen. **26**, 4711 (1993).

[36] John Quintanilla and Robert Ziff, Asymmetry in the percolation thresholds of fully penetrable disks with two different radii, Phys. Rev. E **76**, 051115 (2007).

[37] A. C. Balram and Deepak Dhar, Scaling relation for determining the critical threshold for continuum percolation of overlapping discs of two sizes, Pramana **74**, 109 (2010).

[38] V. Sasidevan, Continuum percolation of overlapping disks with a distribution of radii having a power-law tail, Phys. Rev. E **88**, 022140 (2013).

[39] R. Consiglio, D. R. Baker, G. Paul, and H. E. Stanley, Continuum percolation thresholds for mixtures of spheres of different sizes, Physica A **319**, 49 (2003).

[40] Deepak Dhar, On the critical density for continuum percolation of spheres of variable radii, Physica A **242**, 341 (1997).

[41] D. P. Bentz and E. J. Garboczi, Percolation of phases in a three-dimensional cement paste microstructural model, Cem. Concr. Res. **21**, 325 (1991).

[42] R. Meester, R. Roy, and A. Sarkar, Nonuniversality and continuity of the critical covered volume fraction in continuum percolation, J. Stat. Phys. **75**, 123 (1994).

[43] E. J. Garboczi, K. A. Snyder, J. F. Douglas, and M. F. Thorpe, Geometrical percolation threshold of overlapping ellipsoids, Phys. Rev. E **52**, 819 (1995).

[44] R. M. Ziff, Spanning Probability in 2D Percolation, Phys. Rev. Lett. **69**, 2670 (1992).

[45] R. Consiglio, R. N. A. Zouain, D. R. Baker, G. Paul, and H. E. Stanley, Symmetry of the continuum percolation threshold in systems of two different size objects, Physica A **343**, 343 (2004).

[46] Kelsey Meeks, Michelle L. Pantoya, Micah Green, and Jordan Berg, Extending the excluded volume for percolation threshold estimates in polydisperse systems: The binary disk system, Sandia Technical Report No. 2016-12468J (2016).